OPEN ACCESS

University of BRISTOL

Campana, M-A., Ouisse, M., Sadoulet-Reboul, E., Ruzzene, M., Neild, S. A., & Scarpa, F. (2020). Impact of non-linear resonators in periodic structures using a perturbation approach. *Mechanical Systems and Signal Processing*, *135*, [106408].

Peer reviewed version

License (if available):
CC BY-NC-ND

Link to publication record in Explore Bristol Research
PDF-document

This is the author accepted manuscript (AAM). The final published version (version of record) is available online via Elsevier at https://www.sciencedirect.com/science/article/pii/S0888327019306296?via%3Dihub. Please refer to any applicable terms of use of the publisher.

University of Bristol - Explore Bristol Research
General rights

This document is made available in accordance with publisher policies. Please cite only the published version using the reference above. Full terms of use are available:
http://www.bristol.ac.uk/red/research-policy/pure/user-guides/ebr-terms/

Impact of non-linear resonators in periodic structures using a perturbation approach

M.A. Campana[a,c], M. Ouisse[c], E. Sadoulet-Reboul[c], M. Ruzzene[d], S. Neild[a,b], F. Scarpa[a,b]

[a] *Bristol Composite Institute, University of Bristol, Bristol BS8 1TR, UK*
[b] *Dynamics and Control Research Group (DCRG), Civil. Aerospace and Mechanical Engineering (CAME), University of Bristol, BS8 1TR Bristol, UK*
[c] *Univ. Bourgogne Franche-Comté, FEMTO-ST Department of Applied Mechanics, CNRS/UFC/ENSMM/UTBM, Besançon 25000, FR*
[d] *School of Aerospace Engineering, Georgia Institute of Technology, Atlanta GA 30332, USA*

Abstract

The work describes the wave propagation in a periodic structure formed by a linear spring-mass chain with local Duffing non-linear resonators. The wave propagation is studied using the Floquet-Bloch theorem combined with a perturbation approach to identify the dispersion relations in the nonlinear periodic structure. The theoretical model is benchmarked by a numerical model that considers an analogous finite resonant spring-mass system. The numerical non-linear model provides an apparent dispersion relation of the structure obtained from an inverse identification method, the latter based on imposing a wave number as an initial condition, and then obtaining the corresponding frequency from the analysis of the chain amplitude in the time domain. The perturbation and the numerical methods are compared to discuss the behaviour of the wave propagation in the nonlinear resonators periodic chain. The perturbation is then compared with the Harmonic Balance Method previously used in the literature.

Keywords: Periodic structures, Resonators, Non-linearities

1. Introduction

The Floquet-Bloch theorem is widely used to investigate the wave propagation in periodic structures, initially introduced in mathematics by G. Floquet to analyse the solutions of periodic functions in ordinary differential equations

[1], and then extended to the study of wave propagation in periodic structures [2, 3, 4]. Floquet-Bloch provides the dispersion relation of an assumed infinite periodic structure by analysing the periodic unit cell only. One of the main interests for analysing the wave propagation in these periodic media is to identify "stop bands" or "bandgaps", i.e. frequency areas in which waves are no longer free to propagate. The knowledge of these areas in the wave number/frequency maps can be used to build frequency filters using periodic systems and to create therefore frequency bands in which wave propagation is strongly attenuated. Two types of stop bands can be identified in periodic systems. Bragg bandgaps, related to the material properties or the geometry of the unit cell, using properties like hierarchical structures [5] or auxetic properties [6], and resonant bandgaps, caused by a resonating system included in the periodic structure. In a one dimensional spring-mass resonant system, the combination of a resonating mass with the mass of the principal chain results to an apparent frequency-dependent mass, which has the specificity to become negative for a frequency range close to the eigenfrequency of the resonator. This phenomena is called negative mass effect [7], and is related to the presence of a bandgap in those systems.

Several studies have been performed by using resonators systems in periodic structures. Examples are multi-resonators in a single unit cell [8], or the effect of a graded metamaterial [9] to generate pseudo-periodic systems. A large portion of studies related to wave propagation in periodic arrays (also including damping effects) have been described and reviewed in [10]. Some studies have also focused on beam sandwich structures composed by homogenised continuum media with local resonators [11]. Qian [12] has investigated two-dimensional periodic sandwich plate continuum systems using resonators between the two skin panels. More recent studies are focused on the active control of the resonator to make appear or disappear a bandgap. The article [13] use this concept to create resonators based on temperature-dependant materials, softening the whole structure as the temperature increases to switch the bandgaps to lower frequencies.

Studies about periodic non-linear systems have been performed to observe the effect of the amplitude of the response during wave propagation, and more specifically on the boundaries of the bandgap compared to a linear periodic system. Nonlinear metamaterials have been investigated to see the impact on the dispersion relation using different concepts. Georgiou and Valakis [14] have used a type of oscillator generating nonlinearities from the angle of a pendulum attached to the principal mass of the chain. Other more conventional metamaterial like negative-stiffness structures using bistable element [15] or negative-mass represented by non-linear resonators in a linear periodic chain [16, 17, 18] were studied using the Harmonic Balance Method (HBM) on the relative displacement between the resonant mass and the principal mass of the periodic chain.

The work presented in this paper focuses on developing a formulation to identify the dispersion curve of a non-linear resonator using the perturbation method developed by Nasiretti et al [19] for discrete non-linear spring-mass systems, and then extended to finite element structures by Manktelow et al [20]. The method has been so far applied to full nonlinear periodic systems. Here the behaviour of the nonlinear resonator only is analysed to observe the impact of the eigenfrequency of the resonant system in the corrected term of the dispersion relation. Also, the development of a new numerical inverse method used on a finite periodic chain structure to obtain the dispersion curve is presented and compared with theoretical studies. The method consists in imposing the wave number to the whole chain and then obtain the corresponding frequency analysing the temporal signal obtained after releasing the system. This method is different from usually applied approaches that consist on imposing an excitation and identifying back the wave number [21], and has the particularity to avoid space aliasing as well as control the amplitude we want to impose to be compared with the perturbation technique. In addition, the precise observation of the boundaries of the bandgap can be performed since the wave number is imposed, avoiding the issue of wave number discretisation.

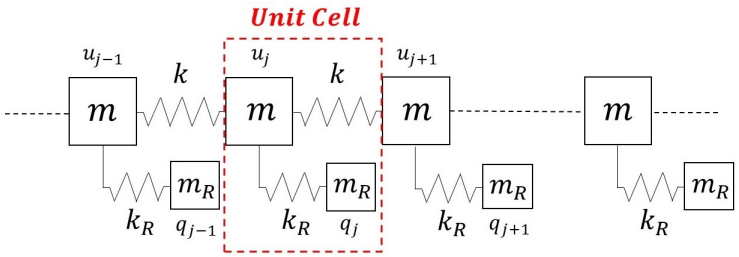

FIGURE 1: 1D resonant spring mass system

2. Dispersion analysis for infinite periodic structures

This section details strategies to determine dispersion relations for infinite periodic structures : the case of a linear spring resonator is first considered, then more attention is dedicated to the case of a nonlinear spring-mass resonator.

2.1. Linear spring-mass resonator

Let consider a one-dimensional principal periodic chain made of spring-mass units (mass m and stiffness k). A resonator represented by another spring-mass system (mass m_R and stiffness k_R) is attached to each mass. This chain is considered as infinite, and an appropriate unit cell is defined to apply the Floquet-Bloch Theorem (Fig. 1).

By writing the equation of motion of the unit cell linked to its neighbours we obtain the following expression :

$$\begin{cases} m\frac{d^2u_j}{dt^2} + k(2u_j - u_{j-1} - u_{j+1}) - k_R(q_j - u_j) = 0 \\ m_R\frac{d^2q_j}{dt^2} + k_R(q_j - u_j) = 0 \end{cases} \tag{1}$$

where u_j and q_j respectively denote the displacements of the j^{th} principal mass and the j^{th} resonating mass. In harmonic regime the displacements can be expressed as $x_j = X_j e^{i\omega t}$, with i being a complex number such as $i^2 = -1$. Eq. 1 becomes :

$$\begin{cases} -\omega^2 m u_j + k(2u_j - u_{j-1} - u_{j+1}) - k_R(q_j - u_j) = 0 \\ -\omega^2 m_R q_j + k_R(q_j - u_j) = 0 \end{cases} \tag{2}$$

The term q_j depends on u_j from the second line of Eq. 2. By applying the Floquet-Bloch Theorem to the first line ($u_{j+1} = e^{j\mu}u_j$, μ being the reduced wave number) one can obtain the following dispersion equation :

$$-m\omega^2 + 2k(1-\cos(\mu)) + (k_R - \frac{k_R^2}{k_R - m_R\omega^2}) = 0 \tag{3}$$

The roots of Eq. 3 are ω_1 and ω_2, representing the two branches of the dispersion curve :

$$\begin{aligned}\omega_1 &= \sqrt{\frac{(m+m_R)\Omega_R^2+4k\sin^2(\mu/2)-\sqrt{((m+m_R)\Omega_R^2+4k\sin^2(\mu/2))^2-16km\sin^2(\mu/2)\Omega_R^2}}{2m}} \\ \omega_2 &= \sqrt{\frac{(m+m_R)\Omega_R^2+4k\sin^2(\mu/2)+\sqrt{((m+m_R)\Omega_R^2+4k\sin^2(\mu/2))^2-16km\sin^2(\mu/2)\Omega_R^2}}{2m}}\end{aligned} \tag{4}$$

with $\Omega_R = \sqrt{\frac{k_R}{m_R}}$ being the eigenfrequency of the resonator. The dispersion curve is shown Fig. 2a, with the propagative part in red and the evanescent part in blue for $m_R = m = 1\ kg$ and $k_R = k = 1\ N.m^{-1}$. To validate numerically the result, a finite spring-mass chain of 20 unit cells has been simulated to obtain the Frequency Response Function (FRF) of the system. The boundary conditions in the numerical model are representative of a free-free state at the two extremities of the chain, while the mass located in one of the ends is excited by imposing a longitudinal propagating wave generated by the force $F(t) = F_0\cos(\omega t)$ with $F_0 = 1N$. An harmonic analysis is performed by varying the value of ω, and the amplitude of the displacement is captured on the mass at the other end of the structure. The results are shown in Fig. 2b.

The FRF exhibits the presence of a frequency region in which the amplitude is considerably attenuated. This area represents the bandgap (resonant in this case). A resonant bandgap can be differentiated from a Bragg one by observing the boundaries of the propagating part [22]. In the resonant case, a wave will stop propagating for a value of $\mu = \pi$ and then propagates again for $\mu = 0$. The boundaries of the bandgap can be expressed by calculating the values of

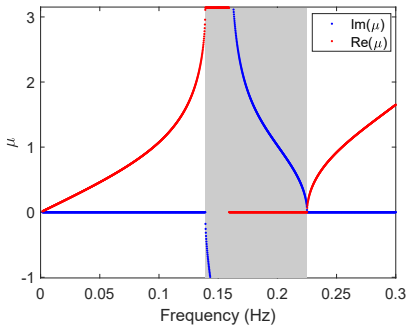

(a) Dispersion curve for the infinite structure. Propagative part in red ($Re(\mu)$) and evanescent part in blue ($Im(\mu)$)

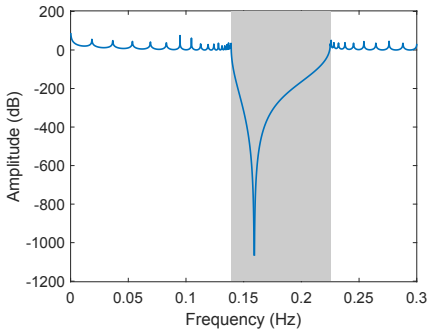

(b) Forced Response Frequency at one of the extremity of a finite structure of 20 unit cells

FIGURE 2: Results for one dimensional linear resonant spring-mass system

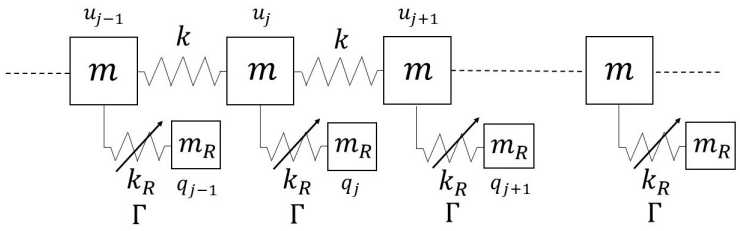

FIGURE 3: 1D non-linear resonant spring mass system

$\omega_1(\mu = \pi)$ and $\omega_2(\mu = 0)$, leading to the following expression :

$$\begin{aligned} \omega_g^2 &= \frac{(m+m_R)\Omega_R^2+4k-\sqrt{((m+m_R)\Omega_R^2+4k)^2-16km\Omega_R^2}}{2m} \\ \omega_d^2 &= \Omega_R^2(1+\tfrac{m_R}{m}) \end{aligned} \tag{5}$$

with ω_g and ω_d being the pulsation of the left and the right boundary, respectively. It is also important to notice that the value of Ω_R is bounded by the values of ω_g and ω_d, and this has consequences on the value of the amplitude of the resonant mass. The rewriting of the second line of Eq. 2 leads to $q_j = \frac{\Omega_R^2}{\Omega_R^2-\omega^2}u_j$, and indicates that the value of the amplitude of q_j strongly depends on the value of Ω_R for a fixed value of the u_j amplitude. The term q_j is bounded in the propagative zone, since $\omega^- < \omega_g < \Omega_R < \omega_d < \omega^+$, with ω^- and ω^+ representing respectively the value of the pulsation before ω_g and after ω_d. This property of a resonating system is different from spring-mass systems with Bragg bandgaps, like the diatomic mass system of Hussein et al. [23]. This particular periodic configuration shows that the amplitudes of the two masses depend directly to the boundaries of the bandgap due to the Bragg effect, which is not the case for the resonating system where the boundaries depend on the value of the eigenfrequency of the resonator, changing the way of evaluating the maximum admissible amplitude to stay in low-level vibration domain.

2.2. Nonlinear spring-mass resonator system

2.2.1. Perturbation method for identification of non-linear dispersion diagram

A Duffing spring mass resonator is added between the masses m and m_R. In this case the non-linear force is expressed as :

$$f_{nl} = k_R(q_j - u_j) + \varepsilon\Gamma(q_j - u_j)^3 \tag{6}$$

where Γ is the nonlinear stiffness constant and ε a small perturbation parameter. Replacing the linear restoring force $-k_R(q_j - u_j)$ by f_{nl} in Eq. 1 leads to :

$$\begin{cases} m\frac{d^2u_j}{dt^2} + k(2u_j - u_{j-1} - u_{j+1}) - k_R(q_j - u_j) - \varepsilon\Gamma(q_j - u_j)^3 = 0 \\ m_R\frac{d^2q_j}{dt^2} + k_R(q_j - u_j) + \varepsilon\Gamma(q_j - u_j)^3 = 0 \end{cases} \tag{7}$$

The objective here is to identify the correction term in the dispersion relation using the Lindstedt-Poincaré adapted method developed in [19]. The main goal is to generate a first order asymptotic development on the displacements of the masses and on the frequency, corresponding to the following expressions :

$$\begin{aligned} u_j &= u_j^{(0)} + \varepsilon u_j^{(1)} + O(\varepsilon^2), \\ q_j &= q_j^{(0)} + \varepsilon q_j^{(1)} + O(\varepsilon^2), \\ \omega &= \omega_0 + \varepsilon\omega_1 + O(\varepsilon^2). \end{aligned} \tag{8}$$

Replacing expressions 8 in Eq. 7 gives, after development and separation of the equations in the ε^0 and ε^1 orders :

$$\varepsilon^0 : \begin{cases} \underline{\omega}_0^2\frac{d^2u_j^{(0)}}{d\tau^2} + (2u_j^{(0)} - u_{j-1}^{(0)} - u_{j+1}^{(0)}) - \beta(q_j^{(0)} - u_j^{(0)}) = 0, \\ \kappa^2\underline{\omega}_0^2\frac{d^2q_j^{(0)}}{d\tau^2} + (q_j^{(0)} - u_j^{(0)}) = 0, \end{cases} \tag{9}$$

$$\varepsilon^1 : \begin{cases} \underline{\omega}_0^2\frac{d^2u_j^{(1)}}{d\tau^2} + (2u_j^{(1)} - u_{j-1}^{(1)} - u_{j+1}^{(1)}) - \beta(q_j^{(1)} - u_j^{(1)}) = -2\underline{\omega}_0\underline{\omega}_1\frac{d^2u_j^{(0)}}{d\tau^2} + \bar{\Gamma}(q_j^{(0)} - u_j^{(0)})^3 \\ \kappa^2\underline{\omega}_0^2\frac{d^2q_j^{(1)}}{d\tau^2} + (q_j^{(1)} - u_j^{(1)}) = -2\kappa^2\underline{\omega}_0\underline{\omega}_1\frac{d^2q_j^{(0)}}{d\tau^2} - \frac{\bar{\Gamma}}{\beta}(q_j^{(0)} - u_j^{(0)})^3 \end{cases} \tag{10}$$

with $\underline{\omega}_n^2 = \frac{\omega_n^2}{\Omega_0^2}$ $(n = 0, 1)$, $\Omega_0^2 = \frac{k}{m}$, $\alpha = \frac{m_R}{m}$, $\beta = \frac{k_R}{k}$, $\kappa = \sqrt{\frac{\alpha}{\beta}}$, $\bar{\Gamma} = \frac{\Gamma}{k}$, $\tau = \omega t$. Assuming an harmonic regime is reached, the displacements $u_j^{(0)}$ and $q_j^{(0)}$ can be expressed in the following form :

$$\begin{aligned} u_j^{(0)} &= \tfrac{A_u}{2} e^{ji\mu} e^{i\tau} + \tfrac{\bar{A}_u}{2} e^{-ji\mu} e^{-i\tau} \\ q_j^{(0)} &= \tfrac{A_q}{2} e^{ji\mu} e^{i\tau} + \tfrac{\bar{A}_q}{2} e^{-ji\mu} e^{-i\tau} \end{aligned} \tag{11}$$

The second order derivatives are then :

$$\begin{aligned} \tfrac{d^2 u_j^{(0)}}{d\tau^2} &= -u_j^{(0)} \\ \tfrac{d^2 q_j^{(0)}}{d\tau^2} &= -q_j^{(0)} \end{aligned} \tag{12}$$

Replacing Eq. 11 and 12 into Eq. 9 yields

$$\varepsilon^0 : \begin{cases} -\underline{\omega}_0^2 u_j^{(0)} + (2u_j^{(0)} - u_{j-1}^{(0)} - u_{j+1}^{(0)}) - \beta(q_j^{(0)} - u_j^{(0)}) = 0 \\ -\kappa^2 \underline{\omega}_0^2 q_j^{(0)} + (q_j^{(0)} - u_j^{(0)}) = 0 \end{cases} \tag{13}$$

Eq. 13 is equivalent to Eq. 2. Following the same process as in the linear case, roots are now expressed as

$$\begin{aligned} (\underline{\omega}_0^{(1)})^2 &= \tfrac{1+\alpha+4\kappa^2 \sin^2(\frac{\mu}{2}) - \sqrt{(1+\alpha+4\kappa^2 \sin^2(\frac{\mu}{2}))^2 - 16\kappa^2 sin^2(\frac{\mu}{2})}}{2\kappa^2}, \\ (\underline{\omega}_0^{(2)})^2 &= \tfrac{1+\alpha+4\kappa^2 \sin^2(\frac{\mu}{2}) + \sqrt{(1+\alpha+4\kappa^2 \sin^2(\frac{\mu}{2}))^2 - 16\kappa^2 sin^2(\frac{\mu}{2})}}{2\kappa^2}. \end{aligned} \tag{14}$$

When adopting the same approach used during the linear analysis, the purpose is to isolate the corrected displacement $q_j^{(1)}$ in the second line of Eq. 10 and inject it in the first line. In this way one can obtain all the nonlinear terms in the same equation. To do so, it is assumed that the displacement $q_j^{(1)}$ can be expressed under the form :

$$q_j^{(1)} = Be^{i\tau} + \bar{B}e^{-i\tau} \tag{15}$$

Where B is the amplitude of $q_j^{(1)}$, whose the value does not have importance for the following calculations. Replacing Eq. 15 in the second line of Eq. 10 we

obtain :

$$\varepsilon^1 : \begin{cases} \underline{\omega}_0^2 \frac{d^2 u_j^{(1)}}{d\tau^2} + (2u_j^{(1)} - u_{j-1}^{(1)} - u_{j+1}^{(1)}) - \beta(q_j^{(1)} - u_j^{(1)}) = -2\underline{\omega}_0\underline{\omega}_1 \frac{d^2 u_j^{(0)}}{d\tau^2} + \bar{\Gamma}(q_j^{(0)} - u_j^{(0)})^3 \\ q_j^{(1)} = \frac{1}{1-\kappa^2\underline{\omega}_0^2}(u_j^{(1)} - 2\kappa^2\underline{\omega}_0\underline{\omega}_1 \frac{d^2 q_j^{(0)}}{d\tau^2} - \frac{\bar{\Gamma}}{\beta}(q_j^{(0)} - u_j^{(0)})^3) \end{cases} \tag{16}$$

Injecting expression of $q_j^{(1)}$ in the first line of Eq. 16 leads to :

$$\underline{\omega}_0^2 \frac{d^2 u_j^{(1)}}{d\tau^2} + (2u_j^{(1)} - u_{j-1}^{(1)} - u_{j+1}^{(1)}) - \beta \frac{\kappa^2\underline{\omega}_0^2}{1-\kappa^2\underline{\omega}_0^2} u_j^{(1)} = F(\tau) \tag{17}$$

with :

$$F(\tau) = 2\underline{\omega}_0\underline{\omega}_1 \frac{\alpha + (1-\kappa^2\underline{\omega}_0^2)^2}{(1-\kappa^2\underline{\omega}_0^2)^2} u_j^{(0)} - \bar{\Gamma}\left(\frac{\kappa^2\underline{\omega}_0^2}{1-\kappa^2\underline{\omega}_0^2}\right)^4 (u_j^{(0)})^3 \tag{18}$$

Replacing $u_j^{(0)}$ by its expression 11, the equation becomes :

$$F(\tau) = \left(\underline{\omega}_0\underline{\omega}_1 \frac{\alpha + (1-\kappa^2\underline{\omega}_0^2)^2}{(1-\kappa^2\underline{\omega}_0^2)^2} A_u - \frac{3\bar{\Gamma}}{8}\left(\frac{\kappa^2\underline{\omega}_0^2}{1-\kappa^2\underline{\omega}_0^2}\right)^4 A_u^2 \bar{A}_u\right) e^{i\tau} e^{ij\mu} + d_1 e^{3i\tau} e^{3ij\mu} \tag{19}$$

The terms d_1 are associated to the 3^{rd} order of the nonlinearity. The linear kernel of Eq. 17 is similar to the one in Eq. 3 ; this implies that one needs to have all the coefficients in $e^{ij\mu}$ be equal to 0 not to obtain a secular term in the temporal expression of $u_j^{(1)}$. By imposing this condition and rearranging the equation, we obtain the following expression for $\underline{\omega}_1$:

$$\underline{\omega}_1 = \frac{3\bar{\Gamma}|A_u|^2}{8} \frac{\kappa^8\underline{\omega}_0^7}{(1-\kappa^2\underline{\omega}_0^2)^2(\alpha + (1-\kappa^2\underline{\omega}_0^2)^2)} \tag{20}$$

Equation 21 leads to the establishment of the final expression describing the corrected dispersion relation for the periodic structure :

$$\underline{\omega} = \underline{\omega}_0 + \varepsilon \frac{3\bar{\Gamma}|A_u|^2}{8} \frac{\kappa^8\underline{\omega}_0^7}{(1-\kappa^2\underline{\omega}_0^2)^2(\alpha + (1-\kappa^2\underline{\omega}_0^2)^2)} \tag{21}$$

Eq. 21 illustrates the importance of the pulsation of the resonator to determine the value of ω_1. If $\kappa^2\underline{\omega}_0^2$ approaches 1 (i.e., equivalent to say that ω

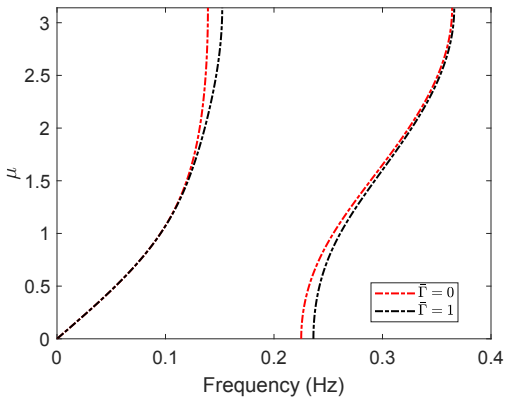

FIGURE 4: Dispersion curve using the perturbation approach in the nonlinear case for $A_u = 1$ and $\varepsilon = 0.05$

approaches the resonance Ω_R), the value of $\underline{\omega}_1$ will increase and might reach a point where it becomes greater than $\underline{\omega}_0$. This would however contradict the hypothesis underlying the current perturbation method.

For the following analyses, the parameters α,κ, $\bar{\Gamma}$ are considered to be equal to 1 (unless $\bar{\Gamma} = 0$, and this to obtain the linear case). A graphic representation of the corrected dispersion curve considering $A_u = 1$ is shown Fig. 4.

2.2.2. Domain of amplitude validity

The perturbation analysis assumes an asymptotic development of the term $\underline{\omega}$ to obtain the nonlinear corrected result. However, the asymptotic development of the term $\underline{\omega}^2 = (\underline{\omega}_0 + \varepsilon\underline{\omega}_1)^2 = \underline{\omega}_0^2 + 2\varepsilon\underline{\omega}_0\underline{\omega}_1$ leading to Eq. 10 is true only if $2\varepsilon\underline{\omega}_0\underline{\omega}_1 \ll \underline{\omega}_0^2$ i.e. $2\varepsilon\frac{\underline{\omega}_1}{\underline{\omega}_0} \ll 1$. $\underline{\omega}_1$ is replaced by its expression 20 leading to the following condition :

$$\frac{3|A_u|^2\varepsilon}{4}\frac{\underline{\omega}_0^6}{(1-\underline{\omega}_0^2)^2(1+(1-\underline{\omega}_0^2)^2)} \ll 1 \tag{22}$$

By assuming that the order of magnitude of $\ll$ is the same as ε, the following

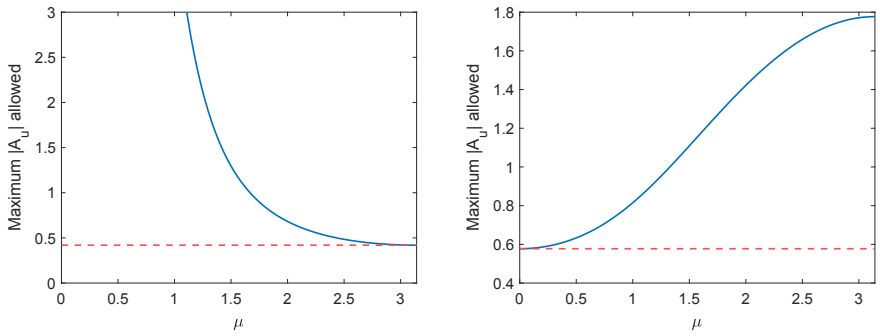

(a) Value of $\frac{1}{h(\underline{\omega}_0)}$ for the left branch of the dispersion curve ($\underline{\omega}_0^{(1)}$)

(b) Value of $\frac{1}{h(\underline{\omega}_0)}$ for the right branch of the dispersion curve ($\underline{\omega}_0^{(2)}$)

FIGURE 5: Maximum of amplitude versus wave number analysis

condition for the amplitude can be written :

$$|A_u| h(\underline{\omega}_0) < 1 \tag{23}$$

where $h(\underline{\omega}_0) = \sqrt{\frac{3}{4} \frac{\underline{\omega}_0^6}{(1-\underline{\omega}_0^2)^2(1+(1-\underline{\omega}_0^2)^2)}}$. Plotting the function $\frac{1}{h}$ will give the maximum admissible value that $|A_u|$ can assume to satisfy the equation 23. The results are shown figure 5. Fig. 5a shows that for values of μ up to 1.0, almost any value of $|A_u|$ would not affect the dispersion in the nonlinear regime. This means that the hypothesis of linearisation in this area remains true even for very high values of amplitude. However, the admissible amplitude results to be much lower when the wave number increases, approaching a maximum theoretical limit of 0.48. The opposite behaviour however happens in the right branch (Fig. 5b) ; in this case it is possible to observe a limit for $|A_u|$, with a minimum value around 0.6 for $\mu = 0$ and reaching 1.8 for $\mu = \pi$.

3. Identification of dispersion curves from analysis of finite nonlinear periodic structures

This section presents a numerical method to obtain the apparent wave number of the structure, followed then by results related to this approach and a

comparison with the method described in 2 and previous methods used in literature such as harmonic analysis and Harmonic Balance Method.

3.1. Inverse method

In general the techniques used to identify the apparent wave number of a periodic structure are based on applying an harmonic excitation to one of the masses of the periodic structure and then evaluating the response by measuring the wave number after a certain time.

This paper introduces here another numerical method to compare the results obtained from the theory. The idea underpinning this methodology is to impose the wave number of the whole structure as an initial condition, releasing the system and observing how it evolves in the time to obtain the frequency of the corresponding imposed wave number. One of the advantages of this novel methodology is that a time-domain analysis is required, rather than the space-domain analysis one to obtain the wave number in direct methods [24]. The use of a time-domain analysis helps to reduce the error made due to the spatial discretisation of the periodic structure. In particular for spring-mass systems, the distance between two consecutive masses does not need to be represented in the model, and this allows to fix the element length to unity. According to the Shannon theorem, a minimum of 2 elements per wavelength is necessary to avoid space aliasing. However, to represent a sinusoidal excitation in a correct way, it is common to use at least 6 elements per wavelength, and that condition can not be reached when the wave number exceeds 1. Fig. 6 illustrates this problem by showing the space representation for two different wave numbers. It is however important to note that this method fits mainly to have a representation of an experimental set under numerical simulations, since imposing a fixed shape to the structure as an initial condition is almost impossible in practice.

The finite structure here is represented by an assembly of 300 unit cells in a linear chain. The equation of motion of the finite structure with a free-free boundary condition is written and solved using ODE45 in Matlab. A perfectly matched layer (PML) is also used at the boundaries of the structure to avoid

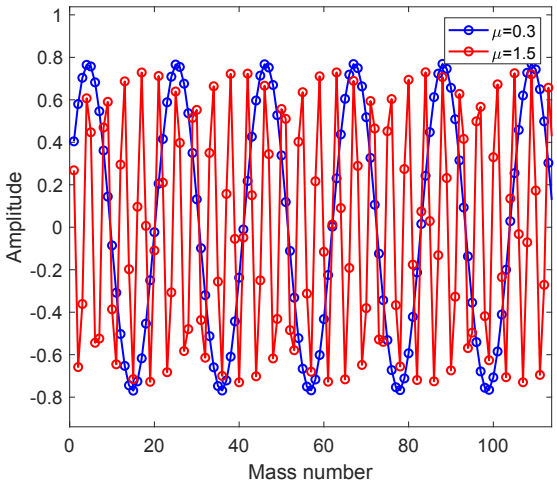

FIGURE 6: Spatial representation of masses for two different values of μ.

wave reflection. The PML consists in a viscous damping force $c(x_p).\dot{x}_p$ applied to all the masses of the principal chain under the form :

$$c(x_p) = Ce^{1-\frac{1}{(1-x_p)^n}} \tag{24}$$

with C a constant positive value, $x_p \in [0;2]$ a value interpolating the mass at the p^{th} position such as $c(0) = c(2) = C$ and $c(1) = 0$, and n an even number representing the order of the PML. The higher the value of n is, the less the masses close to the boundaries will be affected by the damping. Fig. 7 shows the trend of the PML for two different values of n and $C = 2$.

The resolution of the linear system (i.e. with $\Gamma = 0$) has to be done in order to obtain the values of $\underline{\omega}_0(\mu)$ corresponding to the dispersion curve in the linear case. This step is necessary to get the amplitude of the resonating masses as initial condition for the inverse method. Those amplitudes are written as :

$$A_q = \frac{A_u}{1 - \kappa^2 \underline{\omega}_0^2}. \tag{25}$$

Then, the initial conditions applied to the whole structure are written under

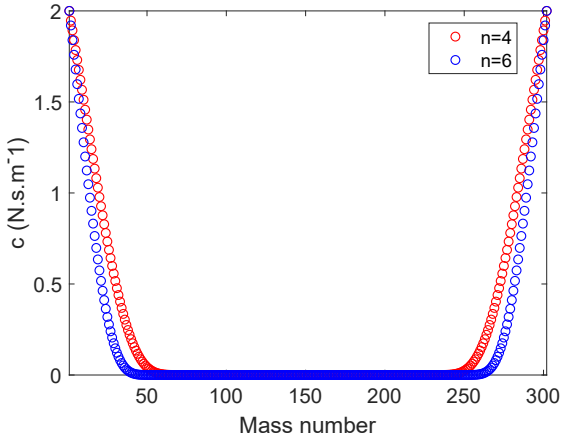

FIGURE 7: Representation of the PML

the following form :

$$\begin{cases} U_j(t=0) = A_u \cos(\mu(x_j - x_0)) \\ \dot{U}_j(t=0) = 0 \\ Q_j(t=0) = A_q \cos(\mu(x_j - x_0)) \\ \dot{Q}_j(t=0) = 0 \\ j \in [\![1; 300]\!] \end{cases} \tag{26}$$

The terms U_j and Q_j are the values of the displacements of the j^{th} principal and resonating mass of the system, respectively. The location of the mass considered to obtain the time-displacement response is x_0. The value of x_0 has to be chosen carefully in order to obtain a coherent representation of the results : if the chosen mass is too close to the boundaries, the PML and eventually residual wave reflections will not give correct values of amplitude. To avoid that issue, observed mass should be located in the middle of the structure. The writing of the initial spatial displacement as in Eq. 26 ensures that the amplitude A_u will be observable for the mass located in x_0 for any value of μ, when $x_j = x_0$. This condition means that the imposed initial displacement is made with a phase shift of $\phi = \mu x_0$, and will not affect the results.

After the masses being released for an imposed wave number μ_0 and a waiting time equivalent to $t = 25T_0$ such as $T_0 = \frac{2\pi}{\omega_0(\mu_0)}$, the frequency of the time signal coming from the mass located in x_0 is measured. One example of input and output signal obtained for a $\mu = 0.1$ on the right branch of the dispersion curve is shown Fig. 9. Fig. 9b shows that the amplitude does not remain constant and equal to A_u as long as the time goes by. Consequently, the Fast Fourier Transform commonly used to get the frequency of a periodic signal would not give accurate results here, since the obtained signal have variations of amplitude and therefore variations of frequency due to the nonlinear behaviour of the resonators. Alternatively, an average of the periods of the signal is done to get the global value of the frequency. Depending on the imposed wave number, the value of the output average amplitude will become different, making not possible a complete comparison with the perturbation method, which assumes a fixed amplitude for every wave number. To fix this problem, an algorithm is implemented, which consists in iterating the simulations starting with an imposed amplitude A_{u_0}. The goal of the algorithm is to reach the targeted value A_u by comparing it with the output amplitude of the system (noted A_{out}). After an iteration, the value of A_{out} is estimated performing a Hilbert transform of the signal :

$$A_{out} = |\mathcal{H}(U_0(t))| \tag{27}$$

If $A_{out} < A_u$, the value of A_{u_0} is slightly increased and the process is repeated until $A_{out} = A_u$ with a certain tolerance. Once this condition is done, one can capture the average frequency of the signal to obtain the combination (μ, ω). A flowchart explaining the algorithm used is given Fig. 8. Fig. 9 shows the results using initial conditions shown in Fig. 10, with a value of $A_{u_0} = 0.53$ to get an average value $A_{out} = 0.5$. The dashed line represents the value of amplitude equal 0.5.

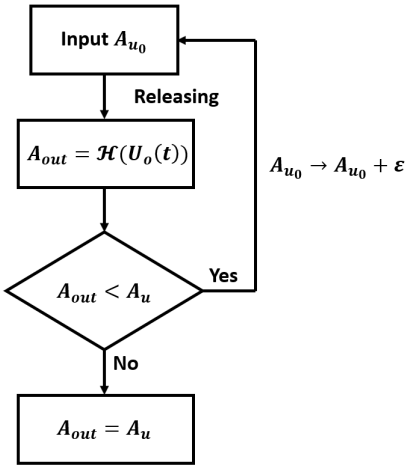

FIGURE 8: Flowchart of the algorithm to get the right amplitude A_{out}

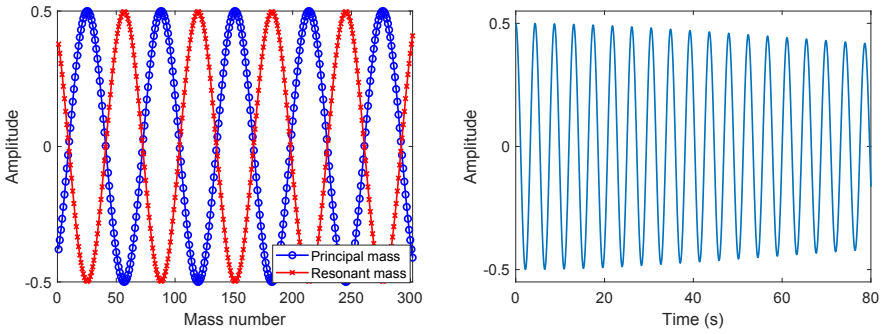

(a) Initial conditions of the system (b) Time signal obtained for the mass x_0

FIGURE 9: Exemple of input and output signal for $A_u = 0.5$ and $\mu = 0.1$

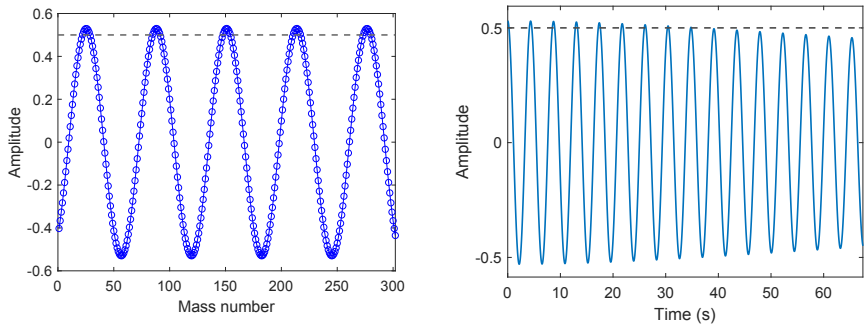

(a) Initial conditions applied to the mass of the principal chain after algorithm

(b) Time signal obtained for the mass x_0 after algorithm

FIGURE 10: Input and output signals obtained after correction

3.2. Numerical results

Before obtaining the numerical nonlinear dispersion curves, a verification of the condition estimated in subsection 2.2.2 has to be performed to verify that the domain of validity of the amplitudes matches with the prediction when using the theoretical model. This verification is done by launching numerical simulations with a variation of the amplitude and the wave number in the following domains : $A_u \in [0.1; 0.6]$, $\mu \in [1; \pi]$ for the left branch and $A_u \in [0.1; 1]$, $\mu \in [0; \pi]$ for the right branch. The values of wave number are not considered in the domain $[0; 1]$ for the left branch since the behaviour of the structure is almost linear in this area even for high values of amplitude as we can see in Fig. 5a. A relative frequency error is calculated as

$$f_{err} = \frac{|f_{num} - f_{per}|}{f_{per}} \tag{28}$$

with f_{num} the frequency obtained with the numerical simulations and f_{per} the frequency obtained with the perturbation method. Also, the value of $2\frac{\omega_0}{\omega_1}$ representing the condition leading to Eq. 23 is calculated. Fig. 11a shows that for high values of μ and amplitudes, the error increases rapidly. Those results generalise what we could observe Fig. 5a, in which the relative error was fixed

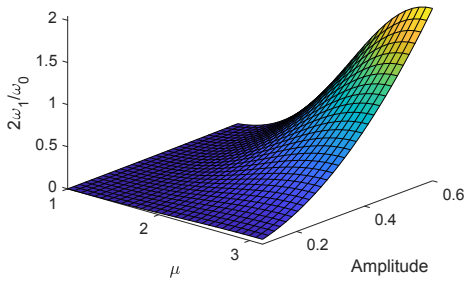

(a) Value of $2\frac{\omega_0}{\omega_1}$ (perturbation method error)

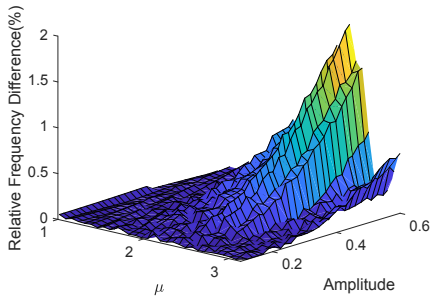

(b) Relative frequency difference between numerical and perturbation method

FIGURE 11: Model error estimation for the left branch of the dispersion curve

to 1, to give an overview of how fast this error is evolving for higher values of amplitude. Fig. 11b shows that the error tends to follow patterns similar to the previous result, and it also shows the same behaviour for high values of amplitude. Similar comments can be provided for the results presented in Fig. 12. In this case, the error also rapidly increases after $A_u \gtrsim 0.3$. Those estimations are close to the ones found with the asymptotic assumption shown in 2.2.2 ; they are however not exactly the same because of the numerical precision of the solver used for the finite structure, and the estimation of taking ε as "small".

The corrected dispersion curve for an amplitude value of $A_u = 0.3$ is repre-

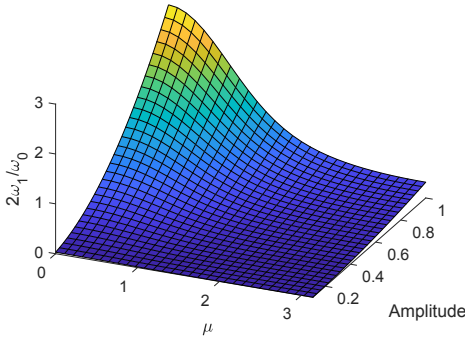

(a) Value of $2\frac{\omega_0}{\omega_1}$ (perturbation method error)

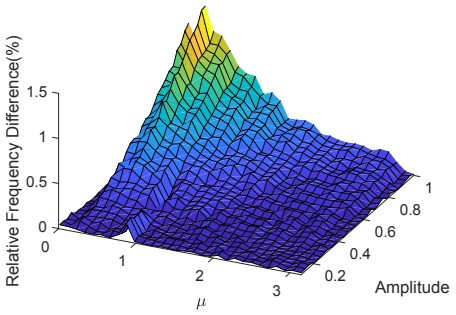

(b) Relative frequency difference between numerical and perturbation method

FIGURE 12: Model error estimation for the right branch of the dispersion curve

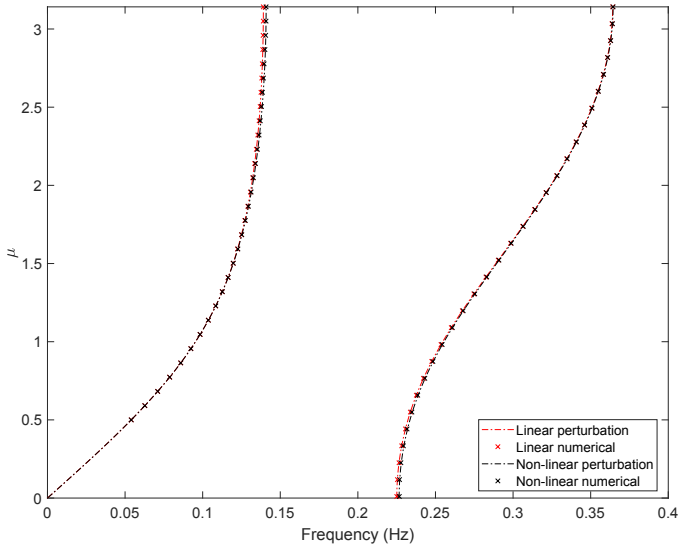

FIGURE 13: Nonlinear dispersion curve ($A_u = 0.3$, $\varepsilon = 0.05$)

sented Fig. 13, and zooms on the branches are shown Fig. 14 and 15. From the close looks it is possible to observe the difference between the numerical method and the perturbation approach. One can observe that for this particular value of amplitude, numerical and theoretical results provide a close match, and the dispersion curve is shifted to higher frequencies compared to the linear case. This result is consistent with the fact that a nonlinear cubic spring has been added to the model, hence stiffening the structure and increasing value of eigenfrequencies. A result imposing an amplitude for an high amplitude ($A_u = 1.5$) and the time signal associated to the value of $\mu = 0.3$ shown Fig. 16. Fig. 16a demonstrates that the results will be inaccurate up to a certain value of wave number (around 0.8 in that case) but will still remain correct after this value. Fig.16b confirms that the perturbation approach will no longer be accurate after a certain value of amplitude.

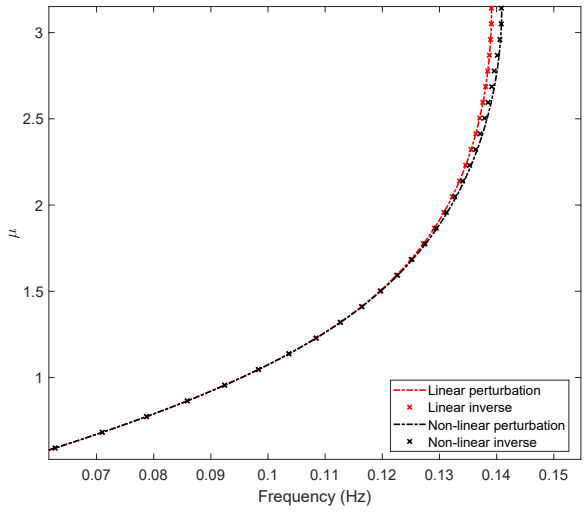

FIGURE 14: Zoom on the left branch of the dispersion curve ($A_u = 0.3$, $\varepsilon = 0.05$)

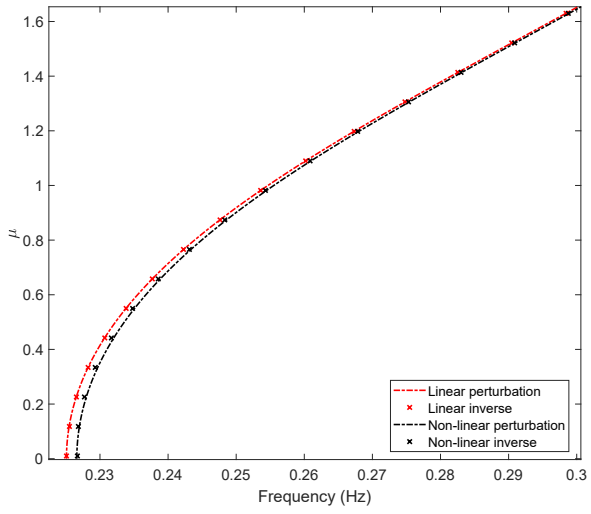

FIGURE 15: Zoom on the right branch of the dispersion curve ($A_u = 0.3$, $\varepsilon = 0.05$)

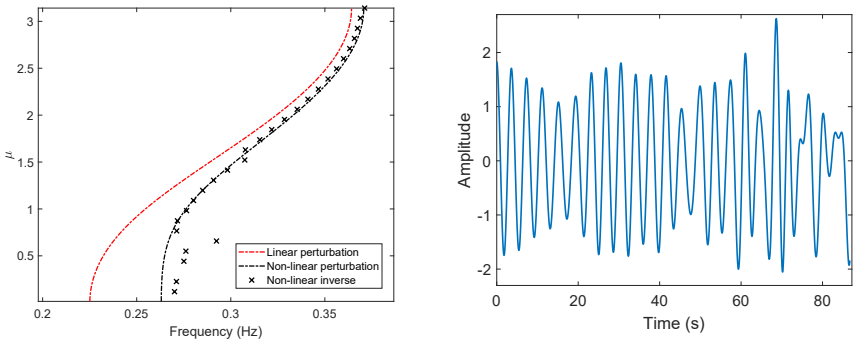

(a) Right branch of the dispersion curve for $A_u = 1.5$

(b) Time signal for $\mu = 0.3$ and a targeted amplitude $A_u = 1.5$

FIGURE 16: Results for an amplitude overpassing the nonlinear assumptions limit

3.3. Comparison with HBM and harmonic analysis

Yet the method presented before give quite accurate results for relatively low values of amplitude, a comparative study is done with previous techniques shown in the literature.

An other way to get the dispersion relation for nonlinear structures is using the Harmonic Balance Method on the relative displacement of the resonant mass according the the principal one [16, 18], noted $v_j = u_j - q_j$. One can assume that v_j can be written under the following form :

$$v_j(\tau) = A_v e^{i\tau} + \bar{A}_v e^{-i\tau} \tag{29}$$

With A_v the amplitude of the relative displacement. Rewriting Eq. 7 taking and using the HBM taking Eq. 29 in consideration leads to a new expression of the dispersion relation of the periodic resonant system given by :

$$\cosh(\mu) = 1 - \frac{\underline{\omega}_0^2}{2} - \frac{\underline{\omega}_0^2 \beta(\kappa^2 + 3\kappa^2 \bar{\Gamma}|A_v|^2)}{2(\kappa^2 + 3\kappa^2 \bar{\Gamma}|A_v|^2 - \underline{\omega}_0^2)} \tag{30}$$

The dispersion relation is here written in the direct form (frequency in input and wave number in output). Using Eq. 25 and knowing that the amplitude of

the relative displacement can be written $A_v = A_q - A_u$, we get :

$$A_v = \frac{\kappa^2 \underline{\omega}_0^2}{1 - \kappa^2 \underline{\omega}_0^2} A_u, \tag{31}$$

meaning that for a constant imposed value of A_u, A_v does not remain constant but varies when the frequency changes. Thanks to Eq. 31, 30 can be used to compare the dispersion curves obtained with the perturbation method and the HBM by imposing a value of amplitude A_u. In addition, an classical harmonic analysis has been performed on the periodic chain presented previously in this section, removing the PML in one of the extremity and applying an harmonic force type $F(t) = F_0 \cos(\omega t)$ at the same extremity. An identification of the wavelength after waiting several periods is then done to be compared with the inverse method. The results of all the different methods are illustrated Fig. 17 for $|A_u| = 0.5$. The perturbation method seems to give slightly better accuracy in this case, since both harmonic analysis and inverse approach are closer to that method compared to the HBM. However, the relative error in frequency between the two methods is relatively small here (about 1%). However, increasing the amplitude to $|A_u| = 1.2$ show that the gap between the perturbation method and the HBM is increasing as shown figure 18 reaching an error about 6%, and giving more accuracy to the perturbation method according to the inverse approach. This seems to show that as the amplitude increase, the perturbation method will give more accurate results than the harmonic balance method, mainly due to the fact that in HBM only the relative displacement is expanded in Fourier series, instead in the perturbation the asymptotic development is both done on the displacements and the frequency, giving a better approximation.

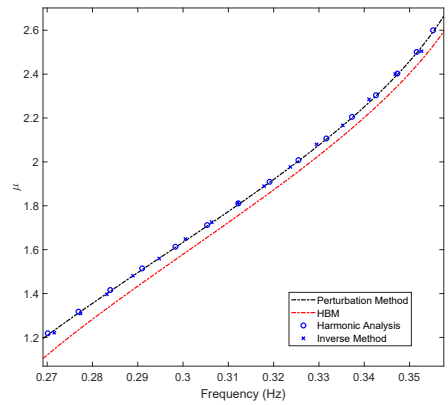

FIGURE 17: Comparison between Perturbation, HBM, inverse approach and harmonic analysis for $|A_u| = 0.5$

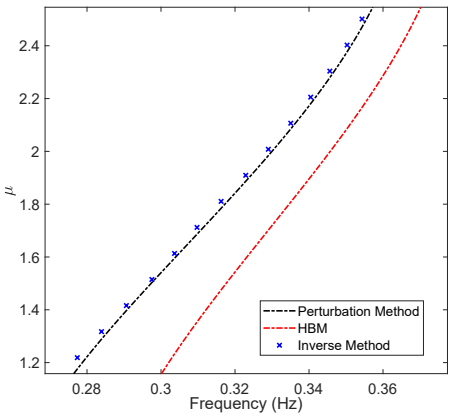

FIGURE 18: Comparison between Perturbation, HBM and inverse approach for $|A_u| = 1.2$

4. Conclusion

Nonlinear periodic resonating systems made of baseline linear chains and distributed Duffing oscillators have been evaluated in this work using a perturbation approach. A quantitative study of the maximum admissible amplitude has been performed to provide an overview of the limits of the proposed method. A new inverse approach imposing the wave number has also been developed and applied to a finite structure with a large number of unit cells to confirm the results obtained with the perturbation method. This numerical inverse identification approach provides a different way of analysing the wave propagation of nonlinear periodic structures. This method can be extended to finite element structures such as unidimensional beams using Floquet eigenvectors as initial conditions for the structure shape before releasing the system taking in consideration geometrical nonlinearities.

5. Acknowledgements

This work has been supported by the MSCA ITN VIPER (Vibroacoustics of Periodic Media) programme.

This project has received funding from the European Union's Horizon 2020 research and innovation programme under Marie Curie grant agreement No 675441.

This work was performed in cooperation with the EUR EIPHI program (ANR 17-EURE-0002).

References

[1] G. Floquet, Sur les équations différentielles linéaires à coefficients périodiques, Annales scientifiques de l'École Normale Supérieure 2e série, 12 (1883) 47–88. doi:10.24033/asens.220.

[2] L. Rayleigh, Xvii. on the maintenance of vibrations by forces of double frequency, and on the propagation of waves through a medium endowed

with a periodic structure, The London, Edinburgh, and Dublin Philosophical Magazine and Journal of Science 24 (147) (1887) 145–159. doi:10.1080/14786448708628074.

[3] L. Brillouin, Wave Propagation in Periodic Structures., Dover Publication, Inc. NY, 1953.

[4] M. Collet, M. Ouisse, M. Ruzzene, M. Ichchou, Floquet–bloch decomposition for the computation of dispersion of two-dimensional periodic, damped mechanical systems, International Journal of Solids and Structures 48 (20) (2011) 2837 – 2848. doi:10.1016/j.ijsolstr.2011.06.002.

[5] K. Billon, I. Zampetakis, F. Scarpa, M. Ouisse, E. Sadoulet-Reboul, M. Collet, A. Perriman, A. Hetherington, Mechanics and band gaps in hierarchical auxetic rectangular perforated composite metamaterials, Composite Structures 160 (2017) 1042–1050. doi:10.1016/j.compstruct.2016.10.121.

[6] M. Ruzzene, L. Mazzarella, P. Tsopelas, F. Scarpa, Wave propagation in sandwich plates with periodic auxetic core, Journal of Intelligent Material Systems and Structures 13 (9) (2002) 587–597. doi:10.1106/104538902031865.

[7] S. Yao, X. Zhou, G. Hu, Experimental study on negative effective mass in a 1d mass–spring system, New Journal of Physics 10 (4) (2008) 043020. doi:10.1088/1367-2630/10/4/043020.

[8] X. Zhou, W. Jun, R. Wang, J. Lin, Effects of relevant parameters on the bandgaps of acoustic metamaterials with multi-resonators, Applied Physics A 122 (2016) 427–434. doi:10.1007/s00339-016-9978-x.

[9] A. Banerjee, R. Das, E. P. Calius, Frequency graded 1d metamaterials : A study on the attenuation bands, Journal of Applied Physics 122 (7) (2017) 1–12. doi:10.1063/1.4998446.

[10] A. Banerjee, R. Das, E. P. Calius, Waves in structured mediums or metamaterials : A review, Archives of Computational Methods in Engineering 25 (2018) 1–30. doi:10.1007/s11831-018-9268-1.

[11] J. Chen, B. Sharma, C. Sun, Dynamic behaviour of sandwich structure containing spring-mass resonators, Composite Structures 93 (8) (2011) 2120 – 2125. doi:10.1016/j.compstruct.2011.02.007.

[12] D. Qian, Z. Shi, Bandgap properties in locally resonant phononic crystal double panel structures with periodically attached spring–mass resonators, Physics Letters A 380 (41) (2016) 3319 – 3325. doi:10.1016/j.physleta.2016.07.068.

[13] K. Billon, M. Ouisse, E. Sadoulet-Reboul, M. Collet, P. Butaud, G. Chevallier, A. Khelif, Design and experimental validation of a temperature-driven adaptive phononic crystal slab, Smart Materials and Structures 28 (3) (2019) 035007. doi:10.1088/1361-665x/aaf670.

[14] I. T. Georgiou, A. F. Vakakis, An invariant manifold approach for studying waves in a one-dimensional array of non-linear oscillators, International Journal of Non-Linear Mechanics 31 (6) (1996) 871 – 886. doi:10.1016/S0020-7462(96)00104-7.

[15] N. Nadkarni, C. Daraio, D. M. Kochmann, Dynamics of periodic mechanical structures containing bistable elastic elements : From elastic to solitary wave propagation, Phys. Rev. E 90 (2014) 023204. doi:10.1103/PhysRevE.90.023204.

[16] B. Lazarov, J. Jensen, Low-frequency band gaps in chains with attached non-linear oscillators, International Journal of Non-Linear Mechanics 42 (10) (2007) 1186 – 1193. doi:10.1016/j.ijnonlinmec.2007.09.007.

[17] X. Fang, J. Wen, B. Bonello, J. Yin, D. Yu, Wave propagation in one-dimensional nonlinear acoustic metamaterials, New Journal of Physics 19 (5) (2017) 053007. doi:10.1088/1367-2630/aa6d49.

[18] K. Wang, J. Zhou, D. Xu, H. Ouyang, Lower band gaps of longitudinal wave in a one-dimensional periodic rod by exploiting geometrical nonlinearity, Mechanical Systems and Signal Processing 124 (2019) 664 – 678. doi:10.1016/j.ymssp.2019.02.008.

[19] R. K. Narisetti, M. Leamy, M. Ruzzene, A perturbation approach for predicting wave propagation in one-dimensional nonlinear periodic structures, Journal of Vibration and Acoustics 132 (2010) 031001–1. doi:10.1115/1.4000775.

[20] K. Manktelow, R. K. Narisetti, M. Leamy, M. Ruzzene, Finite-element based perturbation analysis of wave propagation in nonlinear periodic structures, Mechanical Systems and Signal Processing 39 (2013) 32–46. doi:10.1016/j.ymssp.2012.04.015.

[21] K. L. Manktelow, M. Leamy, M. Ruzzene, Analysis and experimental estimation of nonlinear dispersion in a periodic string, Journal of Vibration and Acoustics 136 (2014) 031016. doi:10.1115/1.4027137.

[22] B. Sharma, C. Sun, Local resonance and bragg bandgaps in sandwich beams containing periodically inserted resonators, Journal of Sound and Vibration 364 (2016) 133 – 146. doi:10.1016/j.jsv.2015.11.019.

[23] M. Hussein, M. Leamy, M. Ruzzene, Dynamics of phononic materials and structures : Historical origins, recent progress, and future outlook, Applied Mechanics Reviews 66 (2014) 040802. doi:10.1115/1.4026911.

[24] J. Berthaut, M. Ichchou, L. Jezequel, K-space identification of apparent structural behaviour, Journal of Sound and Vibration - J SOUND VIB 280 (2005) 1125–1131. doi:10.1016/j.jsv.2004.02.044.